Fibre-optic based particle sensing via deep learning

James A. Grant-Jacob[1]*, Saurabh Jain[1], Yunhui Xie[1], Benita S. Mackay[1], Michael D. T. McDonnell[1], Matthew Praeger[1], Matthew Loxham[2,3], David J Richardson[1], Robert W. Eason[1] and Ben Mills[1]

1 Optoelectronics Research Centre, University of Southampton, Southampton, SO17 1BJ, UK;
2 Academic Unit of Clinical and Experimental Sciences, Faculty of Medicine, University of Southampton, Southampton, SO17 1BJ, UK;
3 NIHR Southampton Biomedical Research Centre, University Hospital Southampton, SO16 6YD, UK;
E-mail: Correspondence: J.A.Grant-Jacob@soton.ac.uk; Tel.: +44-238-059-6975

Abstract

We demonstrate the capability for the identification of single particles, via a neural network, directly from the backscattered light collected by a 30-core optical fibre, when particles are illuminated using a single mode fibre-coupled laser light source. The neural network was shown to be able to determine the specific species of pollen with ~ 97% accuracy, along with the distance between the end of the 30-core sensing fibre and the particles, with an associated error of ± 6 μm. The ability to be able to classify particles directly from backscattered light using an optical fibre has potential in environments in which transmission imaging is neither possible nor suitable, such as sensing over opaque media, in the deep sea or outer space.

Keywords: Deep learning, Fibres, Sensing, Optics, Microparticles, Particle pollution.

Introduction

Fibre-optic based sensors are ideal for worldwide deployment and sensing in a range of in-situ environments owing to their low-cost, light-weight, small and flexible nature. Such fibre sensors can operate in strong electromagnetic fields [1], at high pressures [2], at high temperatures [3] and down to cryogenic temperatures [4], without reduction in sensing performance. In addition, they can operate via single-ended interrogation, such that one end of the fibre can be free to interact like a probe, thus allowing for in-situ sensing in a variety of environments [5]. Sensing examples include areas within stress and strain monitoring in marine and aircraft structures [6,7], landslide detection [8], real-time humidity monitoring [9], hydrogen leak detection from rocket engines [10] and use in the oceans for sea temperature measurements [11].

Particle monitoring in a range of environments is particularly desirable, for example, monitoring the presence and characteristics of plastic microbeads in the sea [12] from cosmetics [13,14] and from the breakdown of larger plastics [15], which can have a demonstrably negative impact on marine life [16–19]. Monitoring of this type can give an indication of the origin and levels of plastic pollution in the marine environment. In air, monitoring of particles, such as those generated by diesel engines, wood burning and pollen, is invaluable for understanding spatiotemporal variation in particulate concentrations, and thus human exposure, which is universally recognised as a current major global health problem. Air pollution (including the effect of gases such as nitrogen oxides) has been associated with increased risk of respiratory and cardiovascular diseases, several cancers, type 2 diabetes mellitus, and dementia [20].

When a particle is illuminated by light, the scattered light encodes information regarding the properties of the particle (such as its refractive index, structure and size) as well as the properties of the surrounding

media in which the particle is immersed [21,22]. It has previously been demonstrated that it is possible to count particles of size < 10 μm, by imaging their scattered light [23]. However, such particle detection systems generally use forward scatter, limiting their use in hard-to-reach environments. Combining particle sensing with fibre optics allows the unique opportunity for backscatter light detection, thereby allowing sensing in environments in which transmission imaging is not possible or suitable.

Deep learning convolutional neural networks [24,25], inspired by the primate visual cortex [26], have gained much interest in the past few years, owing to their ability to classify a vast number of objects, with a certain probability (confidence percentage), that outperforms the capability of humans [27,28]. These types of networks have been implemented in real-time [23] and have been used in areas such as speech recognition [29], facial recognition [30], smile detection [31], video classification [32] and for identifying the songs of different birds [33,34]. The ability to remotely update neural networks without requiring hardware modifications (and with minimal local processing power) is potentially cost effective and advantageous for global distribution [35].

In the field of optics, deep learning has led to classification and predictive capability in laser ablation [36–38], advances in microscopy [39,40], label-free cell classification [41], object classification through scattering media [42–45] and through scattering pattern imaging of plastic microparticles, cells, spores and colloidal particles [46–51]. In the field of fibre-optics, deep learning is gaining interest [52], with work having been reported for perimeter monitoring [53], self-tuning mode-locked fibre lasers [54], and for fibre-optics being used to classify and reconstruct the input handwritten digits and photographs from the speckle patterns transmitted through multimode fibre [55–57]. In addition, deep learning has been used in optical communications [58,59], and more specifically, for real-time fibre mode demodulation [60], end-to-end fibre communications [61], and improvement in fibre transmission [62]. Imaging has also been demonstrated using microstructured fibre [63] and multimode fibre array [64] with deep learning.

Here, we extend on our previous work where deep learning pollution particle detection was carried out using free-space optics [23], and other work showing the capture and analysis of particles in the field using free-space optics [65], by demonstrating the ability to successfully classify real-world bio-aerosol particles (pollen grains) in real-time, via collection of their backscattered light using optical fibres. We show that the neural network can also determine the distance between the pollen particles and the end of the fibres (potentially allowing for 3D mapping), and we examine the robustness of the network by varying the ambient light levels using an additional white light source.

Experimental methods

Sample fabrication: *Iva xanthiifolia* and *Populus deltoides* pollen grains from Sigma Aldrich, and *Narcissus* pollen grains collected from the University of Southampton grounds, were deposited onto a substrate (a 25 mm by 75 mm, 1 mm thick soda-lime glass slide). The pollen grains ranged from ~ 10 to ~ 50 microns in size, and scanning electron microscope images of a selection of the particles are shown in the inset of figure 1. Each pollen type was deposited onto separate region of the glass slide to ensure that the correct labels could be applied during training. The sample was placed on a 3-axis stage (25 mm travel, 10 μm resolution) for positional control.

Imaging setup: As shown in figure 1, light from a diode laser operating at 650 nm was launched into a single mode optical fibre (SMF), while the other end of this illuminating fibre was placed < 100 μm from the pollen coated glass slide, producing a spot size with a diameter of approximately 100 μm. The backscattered light from the particles was collected by a second fibre (referred to here as the sensing fibre). The sensing fibre is a passive multicore fibre (MCF) [66] with 30 cores with 4 different types of core to supress the coupling between cores in long lengths of fibre. The MCF length was < 1 m and, owing to the MCF core structure, intra-core coupling was negligible, potentially allowing higher accuracy for training and testing of the neural networks. However, other fibre bundle designs could

have be used for this sensor. The residual light in the MCF cladding (i.e. not in the cores) was low due to the stripping effect of high index fibre coating applied to the MCF during manufacture. The MCF was placed adjacent and parallel to the fibre light source (the SMF). Light transmitted from the end of the sensing fibre was imaged onto a CMOS colour camera (Thorlabs, DCC3260C, 1936 x 1216 pixels, 10 ms integration time), using a 4 mm focal length lens. The camera was connected to a computer to allow real-time processing via a neural network of the experimentally recorded camera images.

For particle species prediction, the light scattered from a particle varies depending on parameters such as the particle size and type and so the backscattered light from the laser-illuminated pollen, collected by the sensing fibre, also varies accordingly. Examples of these images are shown in figures 1(b)-(d). For the real-time demonstration of particle identification, experimental images were recorded from an area of the sample that was not used for training, but also had separate regions for each type of pollen, so that it was possible to determine if the identification was correct or not. Secondly, for distance prediction, the *Populus deltoides* pollen was used; the glass slide was translated along the z-axis (laser axis) with 200 images recorded at 0 µm, then 200 images recorded 50 µm and so on, at every 50 µm step, for a total distance of 1 mm. Here, half of the recorded images were used for training and validation, and the other half for testing. In order to demonstrate the robustness of this approach, the ambient light level was changed using an additional white light source (a halogen lamp, I. + W. MUSTER Gdb, 150 W) that was directed towards the end of the sensing fibre from the rear of the glass slide, as shown in figure 1. Neutral density filters were placed in front of the source to vary the output level of the additional white light between 0.1% and 100% of the lamp's maximum output. Images of the scattered light transmitted through the sensing fibre were recorded for a total of 10 images per light level, for 11 different light levels and 3 pollen types. These images were trialled on the neural network that was trained with zero additional white light, i.e. only room light, in order to test the robustness of the network to environmental changes, such as light level changes.

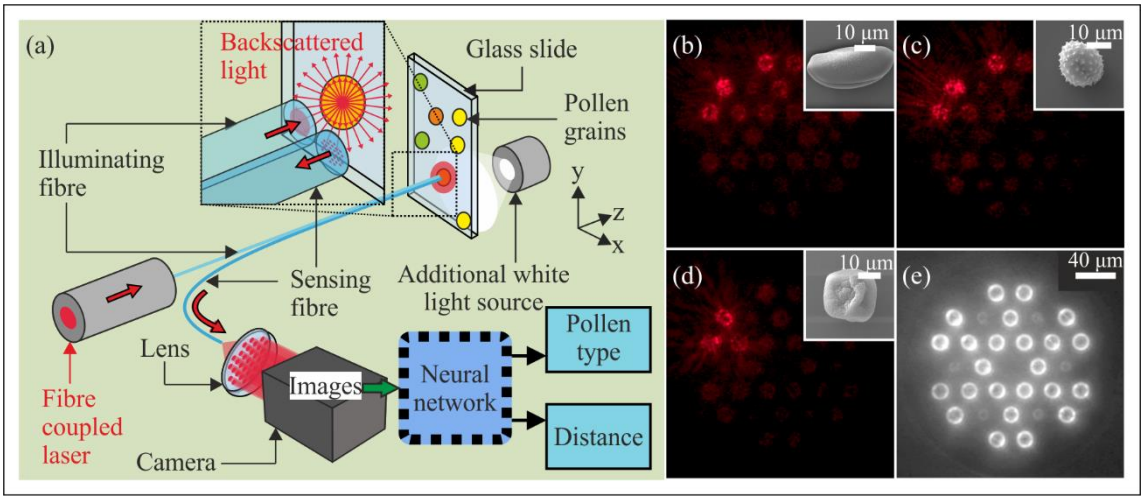

Figure 1. (a) Schematic of setup for backscattered imaging of particles using a SMF for illumination of the particles and a 30-core sensing fibre for collecting the backscattered light. (b)-(d) Example images showing the light collected by the sensing fibre and captured by the camera for *Narcissus, Iva xanthiifolia* and *Populus deltoides* pollen grains, respectively, each with an SEM image inset showing a grain of the corresponding pollen type. (e) Microscope image of the 30-core sensing fibre.

Neural network: A convolutional neural network [27,67] was used and trained on an NVIDIA RTX 5000 graphics processing unit (GPU), with the input as the camera image, and the output was either the particle type (a confidence percentage level for each of the 3 species of pollen) or the distance between the end of the sensing fibre and the particle (a single regression output [68]). Figure 2 shows a simplified schematic of the training procedure of the neural network for the case of identification of the pollen

type. Images of the collected backscattered light were passed into a neural network until the prediction error - comparing the predicted output pollen type with the actual pollen type - was minimised.

More specifically, the images recorded on the camera were cropped to 501 x 501 pixels, resized to 256 x 256 pixels, and then normalised and centred linearly to have a mean of 0 and variance of 1 jointly across all colour channels. The neural network used in this work originated from the second version of ResNet-18 [69] proposed by He et al. [70] (the batch normalisation [71] was used for all networks as a regularisation technique with momentum of 0.95 and mini-batch size of 32). For the classification task (identification of the type of particle), the neural network used was structurally identical to the second version of ResNet-18. In the regression task (predicting the distance between the sensing fibre and the particle), there was only one 1-by-1 filter at the last convolutional layer of the second version of ResNet-18, and hence the output of the regression network was a single number. Deep residual learning (i.e. ResNet) addresses the degradation problem, which appears in many neural network algorithms and can be described as a decrease in proportionality between the depth and the performance of a network when the depth of the network is increased, in deep learning using skip connectivity [70]. This types of structures work reportedly well in many use cases; thus it is chosen for this work. The ResNet-18, as the name stated, used 18 convolutional layers. Apart from the first and the last layer, there were four groups of two connected residual modules, each of which contained two convolutional layers that possessed numbers of 3-by-3 filters. Similar to the idea of stabilising the time complexity between each layer in VGGnet [72], at the first layer on each group, except for the first group, the stride of filters was set to two in order to halve the size of feature maps, whereas the number of filters at all convolutional layers from that group was doubled in comparison with the previous group, which increased the total number of feature maps by a factor of two. The variable initialisation policy followed [73], and the parametric rectifier (PReLU) from the same paper was also adopted to replace the ReLU activation functions [74] used in [69]. The ADAM optimiser [75] was used, with a learning rate of 0.0001. The cost functions used were cross-entropy and mean square error for the classification and regression task respectively. Neither dropout nor L1/L2 regularisation were used in this work. The training time was 5 minutes, and ran for 1 epoch.

The data collection and training were split into two cases; firstly particle identification, and secondly distance prediction. In the first case, across the 3 different types of pollen, a total of 1500 images were collected, 90% of which were used for training and 10% were used for validation of the neural network. For training a neural network for distance prediction, out of the 2200 images collected, 90% were used for training and 10% were used for validation.

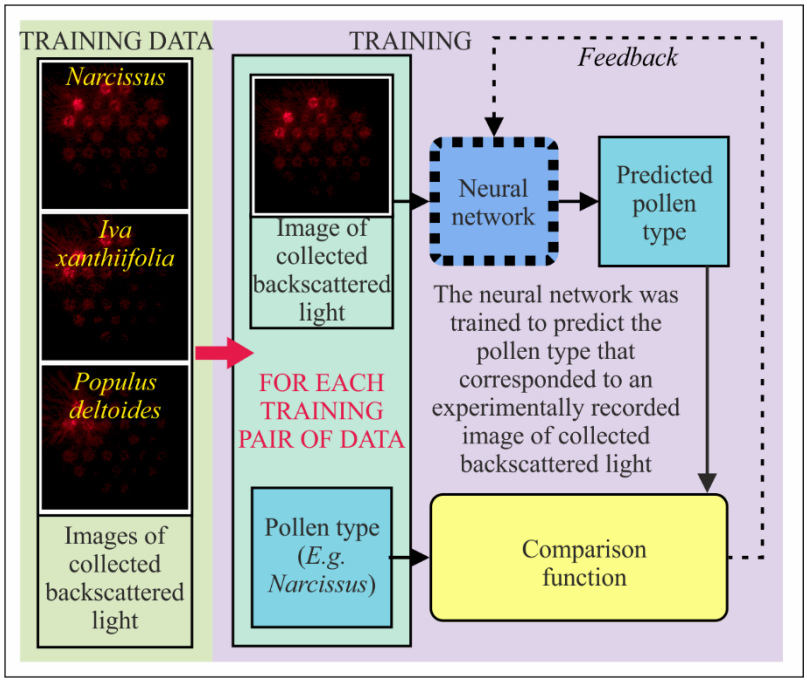

Figure 2. Schematic of neural network training, for the case of identification of the pollen type.

Results and discussion

The results for real-time identification of pollen grain type are shown in figure 3. The inset to figure 3 displays a 10x magnification microscope image indicating the distribution of particles over the surface of the glass slide, showing the variation in size, shape and orientation of the particles. Here, the stage was moved randomly across a region of the sample that was not used when obtaining images for the training data set. When the laser light is incident on a particle, the backscattered light is collected by the camera, inserted into the neural network and a prediction of the pollen type is made. (The pollen type prediction is compared to ground truth via a-priori knowledge of the pollen location on the slide). Out of 30 measurements, 29 predictions were correct (~ 97% accurate, compared with 99.3 % accuracy for the training dataset and 99.9 % for the validation dataset), with a mean confidence percentage for correct prediction of 85.8%. The incorrect measurement was a prediction of *Narcissus*, when the actual pollen type was *Populus deltoides*. This is perhaps due to the variability in the shape of *Populus deltoides* pollen grains, which may have meant that for certain orientation and size, its scattering features appear similar to that of *Narcissus*. Increasing the amount of training data will likely lead to an increase in prediction accuracy of the neural network [76], while increasing the number of light sensing fibres could also increase the amount of the scattered light that is collected (thereby providing a larger effective numerical aperture) and therefore also improve the spatial resolution with which the particles are sampled.

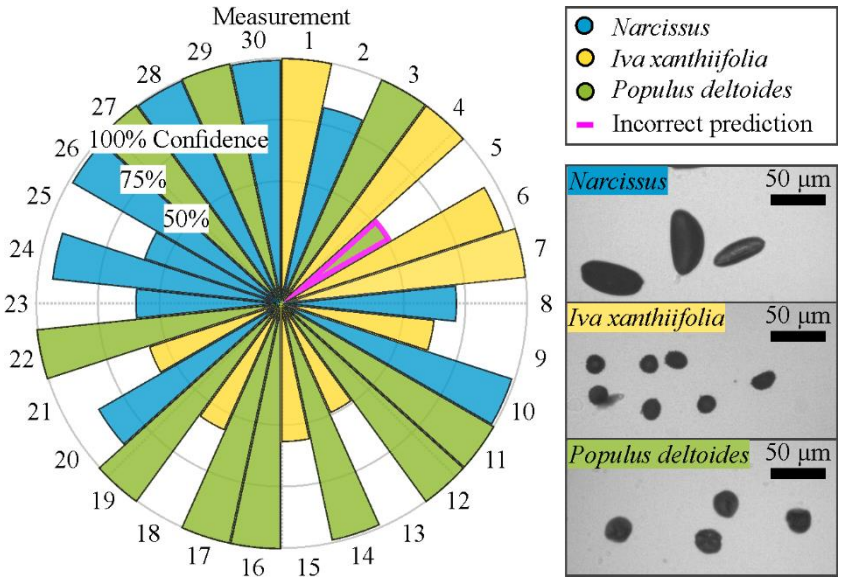

Figure 3. Capability of the trained neural network for predicting the type of pollen, in real-time, for 30 separate predictions, showing the associated confidence percentages. A pink outline indicates an incorrect prediction. Each measurement took 10 milliseconds. Inset: microscope images indicating the variation of pollen grain size, shape and orientation.

As demonstrated in previous work [23], when a neural network is applied to an image of a scattering pattern from a particle that was not observed during training, the neural network will produce a confidence percentage for each of the known particles, based on how closely the scattering pattern from the unknown particle matches features from the scattering patterns from the known particles. In the previous work [23], the neural network, which was trained on forward scattered light from a range of pollen particles, was provided with an image of a scattering pattern from a 5 µm diameter polystyrene microsphere. The neural network produced similar confidence percentages for all known particles (the highest being 46% for the particle type of wood ash), hence implying that scattering pattern from the 5 µm diameter polystyrene microsphere most closely matched the scattering pattern expected from wood ash. As the neural network was not trained on scattering data from polystyrene microspheres, it was incapable of correctly identifying that type of particle.

To extend this discussion, here, we tested the neural network on the collected backscatter from a blank glass slide. Once again, as the neural network was not provided with labelled training data corresponding to the blank glass slide, it was unable to identify this type. Interestingly, in this case, the confidence percentage for a blank glass slide was 99.98% for *Populus deltoides*, hence implying that the features in the scattering pattern from the blank glass slide matched features in the scattering patterns from *Populus deltoides*. This similarity can be observed in figure 4, which shows the light collected by the sensing fibre and captured by the camera for *Narcissus*, *Iva xanthiifolia*, *Populus deltoides* pollen grains and the blank slide, respectively. Some specific regions in the images that are different for the blank slide and *Populus deltoides*, compared with the images for *Narcissus and Iva xanthiifolia*, are highlighted.

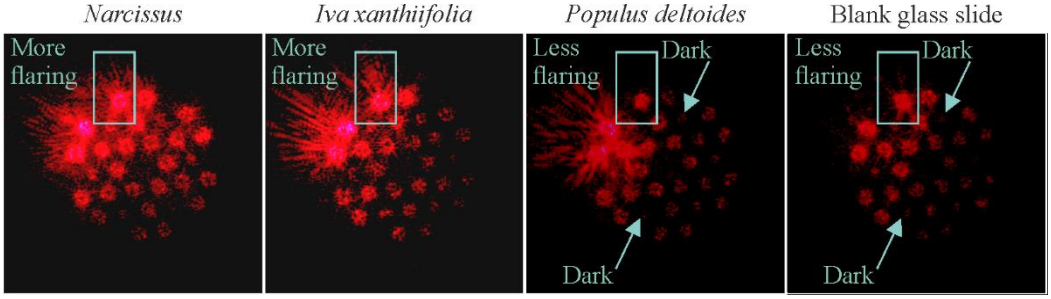

Figure 4. The light collected by the sensing fibre and captured by the camera for *Narcissus, Iva xanthiifolia, Populus deltoides* pollen grains and the blank slide, showing the similarity between the latter two. The brightness and contrast levels of the images have been adjusted equally, compared with the other figures, for ease of analysing.

To minimise the chances of such false identification, a broader range of particles could be used for training, the confidence percentage cut-off for positive identification set high enough, and an unknown category (null category) could be created for the neural network.

The capability for detecting the distance between the end of the sensing fibre and a particle, in combination with the previously demonstrated capability for identification of particle type, offers the potential for simultaneous 3D spatial mapping and identification of particles. Figure 5(a) shows the capability of the trained neural network in determining the distance of the *Populus deltoides* pollen, from the end of the sensing fibre, and (b) shows examples of the collected light imaged on to the camera for 3 different distances. The neural network is shown to be capable of accurately determining the distance, with a standard deviation in the error of ± 6 µm. The method could be extended to further distances, provided that data was collected at those distances and that there was significant signal recorded by the camera. Although the signal-to-noise of the light scattered from the particles would inevitably decrease as the distance is further increased, this could be counteracted by using a more powerful laser beam or adding additional imaging optics onto the end of the fibre.

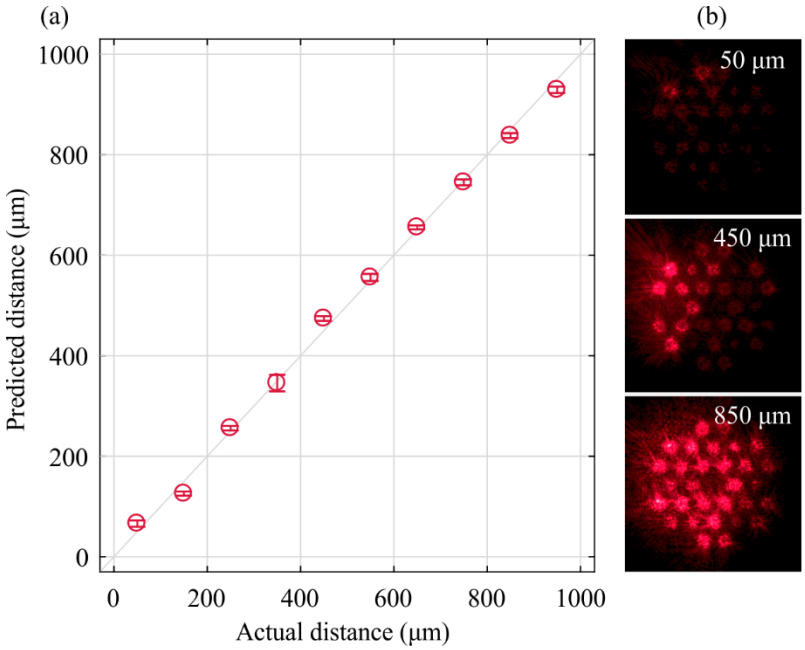

Figure 5. (a) Demonstration of the capability of the trained neural network to predict the distance between the end of the sensing fibre and the *Populus deltoides* pollen, with a standard deviation in the error of ± 6 µm and R-value 0.9976. (b) Examples of camera images showing the collected backscattered light with distances of 50 µm, 450 µm and 850 µm between the end of the sensing fibre and the pollen.

To test the robustness of the neural network under different environmental conditions, and to demonstrate its capability in real-world sensing, a white light source was introduced behind the sample (see figure 1) in order to vary the ambient light levels and thus change the collected backscatter signal; similar in effect to the variation in sunlight throughout the day. The neural network used in this case was the same as that used for figure 3, and hence was trained with zero additional white light, i.e. only room light. Figure 6(a) shows the accuracy of the prediction for the three different types of pollen grain at a fixed position as a function of levels of additional white light. Figure 6(b) shows example images

of the backscattered light from *Narcissus* pollen, illuminated at three different levels of additional white light. The results show that even in illuminance equivalent to that of full daylight, the neural network was still able to identify *Narcissus* and *Iva xanthiifolia*. Interestingly, for *Populus deltoides*, although the confidence percentage decreases at first as the illuminance is increased from low levels of additional white light, it increases again when the level of additional white light is increased from daylight to direct sunlight levels of illuminance and above. This is perhaps due to the wide range of features and signal intensity in the backscattered light images that the neural network associates with each type of pollen. Indeed, when the additional white light at maximum illuminance was directed at the end of the sensing fibre, without laser illumination and in the absence of pollen, the neural network predicted *Populus deltoides* with 100% confidence from the captured image. Whilst the power levels of the white light source used in figure 6 were similar to those in the real-world, the spectrum, and hence colour-balance, of the real-world light sources would depend on the mechanism with which the light was generated. Thus, the neural network accuracy and associated confidence percentages, may be different when using the real-world light sources. To increase the prediction accuracy, the neural network could be trained on varying light levels for each pollen type. For potential sensor applications, environmental conditions are expected to vary, i.e. light levels and colour at dawn may differ considerably from those at midday and ambient temperature may also have an effect. The humidity and the temperature will affect the refractive index of the particles, and hence the scattered light pattern recorded on the camera. With appropriate training data, the neural network could also be applied in order to determine these additional parameters. Additional training data corresponding to different environmental conditions could be created via augmentation of the existing data [77–79], in order to improve accuracy for real-world measurements without the need to collect very large datasets. In addition, to reduce the effects of sunlight, a wavelength filter could be installed in front of the sensor to block out any light that is of a different wavelength to the laser.

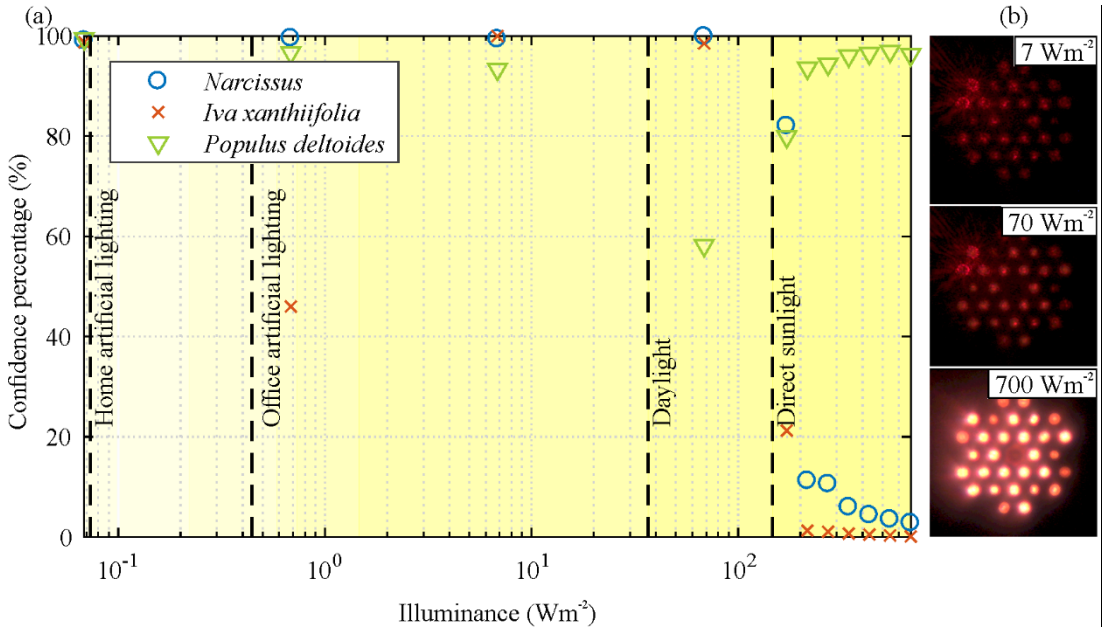

Figure 6. (a) Demonstration of capability of trained neural network for identification of type of pollen grains in the presence of varying levels of additional white light. (b) Example images of backscattered light from *Narcissus* pollen illuminated with additional white light levels of 7 Wm^{-2}, 70 Wm^{-2} and 700 Wm^{-2}. Values of real-world illuminance taken from [80–82].

Conclusion

In conclusion, we have demonstrated a remote, fibre-coupled method for classification of particles, via analysis of their backscattered light. The illumination source is a fibre-coupled laser diode and

backscattered light is collected via a 30-core MCF. The trained neural network was able to identify pollen grain type in real-time, with an accuracy of ~ 97%. The capability for determining the particle distance from the end of the sensing fibre was also demonstrated with an accuracy of ± 6 μm. In addition, the neural network was shown to be robust in the presence of varying ambient white light levels. The combination of these two techniques could allow the simultaneous identification and 3D spatial mapping of particles in challenging and hostile environments.

Acknowledgements

BM was supported by an EPSRC Early Career Fellowship (EP/N03368X/1). ML was supported by a BBSRC Future Leader Fellowship (BB/P011365/1) and a Senior Research Fellowship from the National Institute for Health Research Southampton Biomedical Research Centre. We gratefully acknowledge the support of Fujikura Europe Ltd, who donated the 30-core MCF. Data supporting this manuscript is available at https://doi.org/10.5258/SOTON/D0759

ORCID iDs

James A Grant-Jacob https://orcid.org/0000-0002-4270-4247

Yunhui Xie https://orcid.org/0000-0002-8841-7235

Benita S Mackay https://orcid.org/0000-0003-2050-8912

Matthew Praeger https://orcid.org/0000-0002-5814-6155

Michael D T McDonnell https://orcid.org/0000-0003-4308-1165

Matthew Loxham https://orcid.org/0000-0001-6459-538X

David J Richardson https://orcid.org/0000-0002-4092-6970

Robert W Eason https://orcid.org/0000-0001-9704-2204

Ben Mills https://orcid.org/0000-0002-1784-1012

CONFLICTS OF INTEREST

The authors declare no conflict of interest.

References

[1] Taffoni F, Formica D, Saccomandi P, Pino G Di and Schena E 2013 Optical Fiber-Based MR-Compatible Sensors for Medical Applications: An Overview *Sensors* **13** 14105–20

[2] Kumari C R U, Samiappan D, Kumar R and Sudhakar T 2019 Fiber optic sensors in ocean observation: A comprehensive review *Optik (Stuttg).* **179** 351–60

[3] Roriz P, Frazão O, Lobo-Ribeiro A B, Santos J L and Simões J A 2013 Review of fiber-optic pressure sensors for biomedical and biomechanical applications *J. Biomed. Opt.* **18** 50903

[4] Gupta S, Mizunami T, Yamao T and Shimomura T 1996 Fiber Bragg grating cryogenic temperature sensors *Appl. Opt.* **35** 5202–5

[5] Wang Y and Muth J F 2017 An Optical-Fiber-Based Airborne Particle Sensor *Sensors (Basel).* **17** 2110

[6] Wang G, Pran K, Sagvolden G, Havsgård G B, Jensen A E, Johnson G A and Vohra S T 2001 Ship hull structure monitoring using fibre optic sensors *Smart Mater. Struct.* **10** 472

[7] Qiu J, Li F and Abbas S 2018 A review on SHM techniques and current challenges for characteristic investigation of damage in composite material components of aviation industry *Mater. Perform. Charact.* **7**

[8] Schenato L, Palmieri L, Camporese M, Bersan S, Cola S, Pasuto A, Galtarossa A, Salandin P and Simonini P 2017 Distributed optical fibre sensing for early detection of shallow landslides triggering *Sci. Rep.* **7** 14686

[9] Muto S, Suzuki O, Amano T and Morisawa M 2003 A plastic optical fibre sensor for real-time humidity monitoring *Meas. Sci. Technol.* **14** 746

[10] Bevenot X, Trouillet A, Veillas C, Gagnaire H and Clement M 2000 Hydrogen leak detection using an optical fibre sensor for aerospace applications *Sensors Actuators B Chem.* **67** 57–67

[11] Tyler S W, Selker J S, Hausner M B, Hatch C E, Torgersen T, Thodal C E and Schladow S G 2009 Environmental temperature sensing using Raman spectra DTS fiber-optic methods *Water Resour. Res.* **45**

[12] Rochman C M, Kross S M, Armstrong J B, Bogan M T, Darling E S, Green S J, Smyth A R and Veríssimo D 2015 Scientific Evidence Supports a Ban on Microbeads *Environ. Sci. Technol.* **49** 10759–61

[13] Napper I E, Bakir A, Rowland S J and Thompson R C 2015 Characterisation, quantity and sorptive properties of microplastics extracted from cosmetics *Mar. Pollut. Bull.* **99** 178–85

[14] Cheung P K and Fok L 2016 Evidence of microbeads from personal care product contaminating the sea *Mar. Pollut. Bull.* **109** 582–5

[15] Costa M F, Do Sul J A I, Silva-Cavalcanti J S, Araújo M C B, Spengler Â and Tourinho P S 2010 On the importance of size of plastic fragments and pellets on the strandline: a snapshot of a Brazilian beach *Environ. Monit. Assess.* **168** 299–304

[16] Cózar A, Echevarría F, González-Gordillo J I, Irigoien X, Úbeda B, Hernández-León S, Palma Á T, Navarro S, García-de-Lomas J, Ruiz A, Fernández-de-Puelles M L and Duarte C M 2014 Plastic debris in the open ocean *Proc. Natl. Acad. Sci.* **111** 10239–44

[17] Cole M, Lindeque P, Fileman E, Halsband C, Goodhead R, Moger J and Galloway T S 2013 Microplastic ingestion by zooplankton *Environ. Sci. Technol.* **47** 6646–55

[18] Andrady A L 2011 Microplastics in the marine environment *Mar. Pollut. Bull.* **62** 1596–605

[19] Setälä O, Fleming-Lehtinen V and Lehtiniemi M 2014 Ingestion and transfer of microplastics in the planktonic food web *Environ. Pollut.* **185** 77–83

[20] Holgate S T 2017 “Every breath we take: the lifelong impact of air pollution”--a call for action *Clin. Med. (Northfield. Il).* **17** 8–12

[21] Bohren C F and Huffman D R 2008 *Absorption and scattering of light by small particles* (John Wiley & Sons)

[22] Mills B, Chau C F, Rogers E T F, Grant-Jacob J, Stebbings S L, Praeger M, de Paula A M, Froud C A, Chapman R T, Butcher T J, Baumberg J J, Brocklesby W S and Frey J G 2008 Direct measurement of the complex refractive index in the extreme ultraviolet spectral region using diffraction from a nanosphere array *Appl. Phys. Lett.* **93** 231103

[23] Grant-Jacob J A, Mackay B S, Baker J A G, Heath D J, Xie Y, Loxham M, Eason R W and Mills B 2018 Real-time particle pollution sensing using machine learning *Opt. Express* **26** 27237–46

[24] Szegedy C, Liu W, Jia Y, Sermanet P, Reed S, Anguelov D, Erhan D, Vanhoucke V and Rabinovich A 2015 Going deeper with convolutions *Proceedings of the IEEE conference on computer vision and pattern recognition* pp 1–9

[25] LeCun Y, Bengio Y and Hinton G 2015 Deep learning *Nature* **521** 436

[26] Serre T, Wolf L, Bileschi S, Riesenhuber M and Poggio T 2007 Robust object recognition with cortex-like mechanisms *IEEE Trans. Pattern Anal. Mach. Intell.* 411–26

[27] Krizhevsky A, Sutskever I and Hinton G E 2012 Imagenet classification with deep convolutional neural networks *Advances in neural information processing systems* pp 1097–105

[28] Simonyan K and Zisserman A 2014 Very deep convolutional networks for large-scale image recognition *arXiv Prepr. arXiv1409.1556*

[29] Qian Y, Bi M, Tan T and Yu K 2016 Very deep convolutional neural networks for noise robust speech recognition *IEEE/ACM Trans. Audio, Speech, Lang. Process.* **24** 2263–76

[30] Mollahosseini A, Chan D and Mahoor M H 2016 Going deeper in facial expression recognition using deep neural networks *2016 IEEE winter conference on applications of computer vision (WACV)* pp 1–10

[31] Chen J, Ou Q, Chi Z and Fu H 2017 Smile detection in the wild with deep convolutional neural networks *Mach. Vis. Appl.* **28** 173–83

[32] Karpathy A, Toderici G, Shetty S, Leung T, Sukthankar R and Fei-Fei L 2014 Large-scale video classification with convolutional neural networks *Proceedings of the IEEE conference on Computer Vision and Pattern Recognition* pp 1725–32

[33] Fazeka B, Schindler A, Lidy T and Rauber A 2018 A multi-modal deep neural network approach to bird-song identification *arXiv Prepr. arXiv1811.04448*

[34] Joly A, Goëau H, Glotin H, Spampinato C, Bonnet P, Vellinga W-P, Champ J, Planqué R, Palazzo S and Müller H 2016 LifeCLEF 2016: multimedia life species identification challenges *International Conference of the Cross-Language Evaluation Forum for European Languages* pp 286–310

[35] Achille A, Eccles T, Matthey L, Burgess C P, Watters N, Lerchner A and Higgins I 2018 Life-Long Disentangled Representation Learning with Cross-Domain Latent Homologies *arXiv Prepr. arXiv1808.06508*

[36] Heath D J, Grant-Jacob J A, Xie Y, Mackay B S, Baker J A G, Eason R W and Mills B 2018 Machine learning for 3D simulated visualization of laser machining *Opt. Express* **26** 4984–8

[37] Mills B, Heath D J, Grant-Jacob J A and Eason R W 2018 Predictive capabilities for laser machining via a neural network *Opt. Express* **26** 17245–53

[38] Mills B, Heath D J, Grant-Jacob J A, Xie Y and Eason R W 2018 Image-based monitoring of femtosecond laser machining via a neural network *J. Phys. Photonics* **1** 15008

[39] Rivenson Y, Göröcs Z, Günaydin H, Zhang Y, Wang H and Ozcan A 2017 Deep learning microscopy *Optica* **4** 1437–43

[40] Rivenson Y, Zhang Y, Günaydin H, Teng D and Ozcan A 2018 Phase recovery and holographic image reconstruction using deep learning in neural networks *Light Sci. Appl.* **7** 17141

[41] Chen C L, Mahjoubfar A, Tai L-C, Blaby I K, Huang A, Niazi K R and Jalali B 2016 Deep Learning in Label-free Cell Classification *Sci. Rep.* **6** 21471

[42] Li S, Deng M, Lee J, Sinha A and Barbastathis G 2017 Imaging through glass diffusers using densely connected convolutional networks *arXiv Prepr. arXiv1711.06810*

[43] Satat G, Tancik M, Gupta O, Heshmat B and Raskar R 2017 Object classification through scattering media with deep learning on time resolved measurement *Opt. Express* **25** 17466–79

[44] Valent E and Silberberg Y 2018 Scatterer recognition via analysis of speckle patterns *Optica* **5** 204–7

[45] Li Y, Xue Y and Tian L 2018 Deep speckle correlation: a deep learning approach toward scalable imaging through scattering media *Optica* **5** 1181–90

[46] Grant-Jacob J A, Xie Y, Mackay B S, Praeger M, McDonnell M D T, Heath D J, Loxham M, Eason R W and Mills B 2019 Particle and salinity sensing for the marine environment via deep learning using a Raspberry Pi *Environ. Res. Commun.* **1** 35001

[47] Dong K, Feng Y, Jacobs K M, Lu J Q, Brock R S, Yang L V, Bertrand F E, Farwell M A and Hu X-H 2011 Label-free classification of cultured cells through diffraction imaging *Biomed. Opt. Express* **2** 1717–26

[48] Lee S-H, Roichman Y, Yi G-R, Kim S-H, Yang S-M, Van Blaaderen A, Van Oostrum P and Grier D G 2007 Characterizing and tracking single colloidal particles with video holographic microscopy *Opt. Express* **15** 18275–82

[49] Perry R W, Meng G, Dimiduk T G, Fung J and Manoharan V N 2012 Real-space studies of the structure and dynamics of self-assembled colloidal clusters *Faraday Discuss.* **159** 211–34

[50] Wang C, Cheong F C, Ruffner D B, Zhong X, Ward M D and Grier D G 2016 Holographic characterization of colloidal fractal aggregates *Soft Matter* **12** 8774–80

[51] Yevick A, Hannel M and Grier D G 2014 Machine-learning approach to holographic particle characterization *Opt. Express* **22** 26884–90

[52] Zibar D, Wymeersch H and Lyubomirsky I 2017 Machine learning under the spotlight *Nat. Photonics* **11** 749

[53] Makarenko A V 2016 Deep learning algorithms for signal recognition in long perimeter monitoring distributed fiber optic sensors *2016 IEEE 26th International Workshop on Machine Learning for Signal Processing (MLSP)* pp 1–6

[54] Baumeister T, Brunton S L and Kutz J N 2018 Deep learning and model predictive control for self-tuning mode-locked lasers *J. Opt. Soc. Am. B* **35** 617–26

[55] Borhani N, Kakkava E, Moser C and Psaltis D 2018 Learning to see through multimode fibers *Optica* **5** 960–6

[56] Wang P and Di J 2018 Deep learning-based object classification through multimode fiber via a CNN-architecture SpeckleNet *Appl. Opt.* **57** 8258–63

[57] Rahmani B, Loterie D, Konstantinou G, Psaltis D and Moser C 2018 Multimode optical fiber transmission with a deep learning network *Light Sci. Appl.* **7** 69

[58] Khan F N, Fan Q, Lu C and Lau A P T 2019 An Optical Communication's Perspective on Machine Learning and Its Applications *J. Light. Technol.* **37** 493–516

[59] Ahmed U, Khan A, Khan S H, Basit A, Haq I U and Lee Y S 2019 Transfer Learning and Meta Classification Based Deep Churn Prediction System for Telecom Industry *arXiv Prepr. arXiv1901.06091*

[60] Gao H, Hu H, Zhao Y and Li J 2019 A real-time fiber mode demodulation method enhanced by convolution neural network *Opt. Fiber Technol.* **50** 139–44

[61] Karanov B, Chagnon M, Thouin F, Eriksson T A, Bülow H, Lavery D, Bayvel P and Schmalen L 2018 End-to-end deep learning of optical fiber communications *J. Light. Technol.* **36** 4843–55

[62] Kotlyar O, Pankratova M, Kamalian M, Vasylchenkova A, Prilepsky J E and Turitsyn S K

2018 Unsupervised and supervised machine learning for performance improvement of NFT optical transmission *2018 IEEE British and Irish Conference on Optics and Photonics (BICOP)* pp 1–4

[63] Zhao J, Sun Y, Zhu Z, Antonio-Lopez J E, Correa R A, Pang S and Schülzgen A 2018 Deep Learning Imaging through Fully-Flexible Glass-Air Disordered Fiber *ACS Photonics* **5** 3930–5

[64] Kürüm U, Wiecha P R, French R and Muskens O L 2019 Deep learning enabled real time speckle recognition and hyperspectral imaging using a multimode fiber array *Opt. Express* **27** 20965–79

[65] Wu Y, Calis A, Luo Y, Chen C, Lutton M, Rivenson Y, Lin X, Koydemir H C, Zhang Y, Wang H and others 2019 Label-free Bio-aerosol Sensing Using On-Chip Holographic Microscopy and Deep Learning *CLEO: Applications and Technology* p AM2K--3

[66] Amma Y, Sasaki Y, Takenaga K, Matsuo S, Tu J, Saitoh K, Koshiba M, Morioka T and Miyamoto Y 2015 High-density multicore fiber with heterogeneous core arrangement *2015 Optical Fiber Communications Conference and Exhibition (OFC)* pp 1–3

[67] Lawrence S, Giles C L, Tsoi A C and Back A D 1997 Face recognition: A convolutional neural-network approach *IEEE Trans. neural networks* **8** 98–113

[68] Specht D F 1991 A general regression neural network *IEEE Trans. neural networks* **2** 568–76

[69] He K, Zhang X, Ren S and Sun J 2016 Identity mappings in deep residual networks *European conference on computer vision* pp 630–45

[70] He K, Zhang X, Ren S and Sun J 2016 Deep residual learning for image recognition *Proceedings of the IEEE conference on computer vision and pattern recognition* pp 770–8

[71] Ioffe S and Szegedy C 2015 Batch normalization: Accelerating deep network training by reducing internal covariate shift *arXiv Prepr. arXiv1502.03167*

[72] Simonyan K and Zisserman A 2015 Very Deep Convolutional Networks for Large-Scale Image Recognition *ICLR 2015 : International Conference on Learning Representations 2015*

[73] He K, Zhang X, Ren S and Sun J 2015 Delving deep into rectifiers: Surpassing human-level performance on imagenet classification *Proceedings of the IEEE international conference on computer vision* pp 1026–34

[74] Agarap A F 2018 Deep learning using rectified linear units (relu) *arXiv Prepr. arXiv1803.08375*

[75] Kingma D P and Ba J 2014 Adam: A method for stochastic optimization *arXiv Prepr. arXiv1412.6980*

[76] Cho J, Lee K, Shin E, Choy G and Do S 2015 How much data is needed to train a medical image deep learning system to achieve necessary high accuracy? *arXiv Prepr. arXiv1511.06348*

[77] Perez L and Wang J 2017 The effectiveness of data augmentation in image classification using deep learning *arXiv Prepr. arXiv1712.04621*

[78] Milletari F, Navab N and Ahmadi S-A 2016 V-Net: Fully Convolutional Neural Networks for Volumetric Medical Image Segmentation *arXiv Prepr. arXiv1606.04797*

[79] Hernández-García A and König P 2018 Do deep nets really need weight decay and dropout? *arXiv* **1802.07042** 1–5

[80] West S 2001 Improving the sustainable development of building stock by the implementation of energy efficient, climate control technologies *Build. Environ.* **36** 281–9

[81] C.Lam J and Li D H W 1996 Luminous efficacy of daylight under different sky conditions *Energy Convers. Manag.* **37** 1703–11

[82] Bowers A R, Meek C and Stewart N 2001 Illumination and reading performance in age-related macular degeneration *Clin. Exp. Optom.* **84** 139–47